First-Principles Molecular Dynamics Investigation of the D-Amino Acid Oxidative Half-Reaction Catalyzed by the Flavoenzyme D-Amino Acid Oxidase[†,‡]

Antonio Tilocca,[§] Aldo Gamba, Maria Antonietta Vanoni, and Ettore Fois*

Dipartimento di Scienze Chimiche, Fisiche e Matematiche, Università dell'Insubria at Como, Via Lucini 3, I-22100 Como, Italy

Received April 25, 2002

ABSTRACT: Large-scale Car−Parrinello molecular dynamics simulations of D-alanine oxidation catalyzed by the flavoenzyme D-amino acid oxidase have been carried out. A model of the enzyme active site was built by starting from the enzyme X-ray structure, and by testing different subsystems comprising different sets of aminoacyl residues. In this process, the stability of the enzyme−substrate complex was taken as a measure of the accuracy of the model. The activated transfer of the amino acid α-hydrogen from the substrate to the flavin N5 position was then induced by constraining a suitable transfer reaction coordinate, and the free energy profile of the reaction was calculated. The evolution of electronic and structural properties of both enzyme-bound substrate and flavin cofactor along the reaction path is consistent with a hydride-transfer mechanism. The calculated free energy barrier for this process (13 kcal/mol) is in excellent agreement with the activation energy value derived from the experimentally determined rate constant for the corresponding enzyme-catalyzed reaction. The electronic distribution of the reduced flavin shows that the transferred electrons tend to be centered near the C4a position rather than delocalized over the flavin pyrimidine ring. This feature is mechanistically relevant in that such an electronic distribution may promote the subsequent enzyme-catalyzed reduction of molecular oxygen to yield hydrogen peroxide via a postulated flavin 4a-peroxide intermediate. These results also show that a first-principles molecular dynamics approach is suitable to study the mechanism of complex enzymatic processes, provided that a smaller, yet reliable, subsystem of the enzyme can be identified, and special computational techniques are employed to enhance the sampling of the reactive event.

The modeling of enzyme−substrate complexes, and, in particular, of reactive processes involving the breaking and forming of chemical bonds as well as many-body, polarization, and hydration effects modifying the electronic distribution during the evolution of the system, is a prohibitive task for molecular dynamics approaches based on empirical, predefined force fields (*1*, *2*). On the other hand, ab initio molecular dynamics simulations based on the Car−Parrinello method (*3*) have proven to give reliable results in the modeling of chemical reactions in condensed phases (*4*−*7*) as well as in highlighting the structure and dynamics in enzymatic systems (*6*, *7*). The first-principles determination of interatomic forces based on density functional theory (DFT;[1] *13*, *14*) allows parameter-free simulations including all the complex effects mentioned above to be performed. The accuracy of DFT theory has been discussed thoroughly in the literature (see, e.g., ref *15*). Recent reviews, focused on ab initio studies of biochemical systems, can be found in refs *16* and *17*, while a discussion on the behavior of current DFT approximations for very weak (dispersion) interactions can be found in ref *18*.

D-Amino acid oxidase (DAAO) is the prototype of flavin adenine dinucleotide (FAD)-containing enzymes of the oxidase class (for recent comprehensive reviews see refs *19*−*22*).

DAAO catalyzes the oxidative deamination of D-amino acids to yield the corresponding α-keto acid and ammonia according to eqs 1−3.

$$RCHNH_2COOH + \text{E-FAD} \rightarrow RC{=}NHCOOH + \text{E-FADH}_2 \quad (1)$$

$$\text{E-FADH}_2 + O_2 \rightarrow \text{E-FAD} + H_2O_2 \quad (2)$$

$$RC{=}NHCOOH + H_2O \rightarrow RCOCOOH + NH_3 \quad (3)$$

In the first reaction (eq 1) the substrate is oxidized to the corresponding imino acid with concomitant reduction of the enzyme-bound flavin cofactor to the hydroquinone form. The latter is oxidized by molecular oxygen (eq 2), yielding hydrogen peroxide and oxidized FAD, thus closing the catalytic cycle. The nonenzymatic hydrolysis of the imino acid (eq 3) then completes the reaction, yielding the α-keto acid and ammonia products.

[†] The calculations performed in this work were partially supported by a grant of computer time from the CINECA Supercomputing Center at Bologna, Italy.

[‡] This paper is dedicated to the memory of Prof. Vincent Massey.

* To whom correspondence should be addressed. Phone: +39 031 326218. Fax: +39 031 326230. E-mail: fois@fis.unico.it.

[§] Present address: Department of Chemistry, Princeton University, Princeton NJ 08544.

[1] Abbreviations: DFT, density functional theory; pk-, Rg-, and Tv-DAAO, D-amino acid oxidase from pig kidney, *Rhodotorula gracilis*, and *Trigonopsis variabilis*, respectively; FAD, flavin adenine dinucleotide; MD, molecular dynamics; TS, transition state; DPC, Δ^1-pyrrolidine-2-carboxylate; CT, charge-transfer complex; WFC, Wannier function centroid.

10.1021/bi020309q CCC: $22.00
Published on Web 11/07/2002

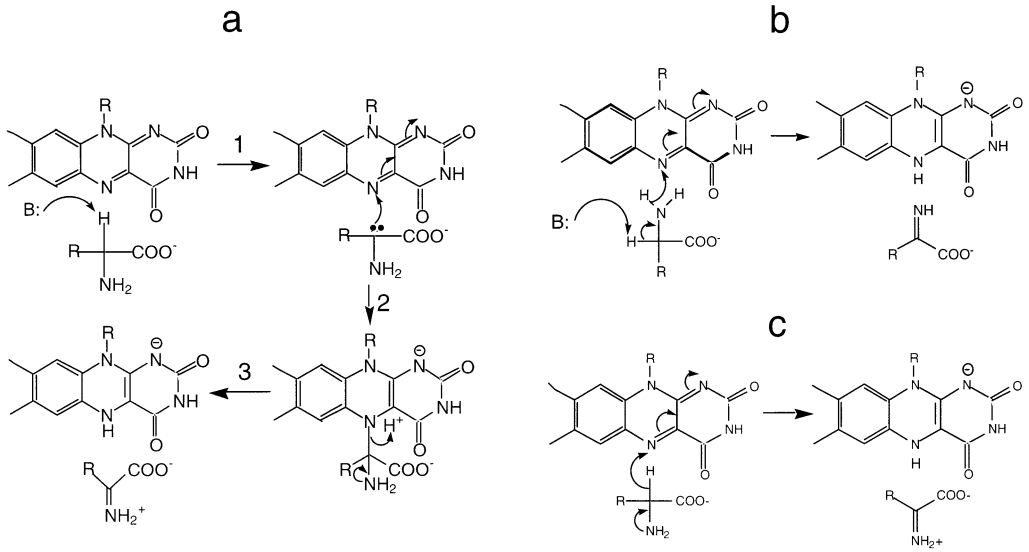

FIGURE 1: Proposed mechanisms for DAAO-catalyzed D-alanine dehydrogenation: (a) carbanion mechanism; (b) hydride transfer from the α-amino group; (c) direct hydride transfer.

A number of kinetic and mechanistic studies have been performed on pig kidney DAAO (pk-DAAO), making it the prototype of flavin-dependent oxidases (*19*−*22*). However, several mechanistic issues have not been solved yet. The mechanism of oxygen reduction to yield hydrogen peroxide (eq 2) is still unknown, while at least three different mechanisms for substrate dehydrogenation (eq 1) have been proposed. As shown in Figure 1, the proposed mechanisms differ for the mode of transfer of two electrons plus one proton to the flavin isoalloxazine nucleus. In the so-called "carbanion mechanism" (Figure 1a) an active site base would abstract the amino acid α-proton, forming a carbanion intermediate (Figure 1a, step 1). Two electrons would be transferred from such a discrete intermediate to the flavin, perhaps through formation of a covalent adduct with the flavin N5 position (Figure 1a, steps 2 and 3). A second hypothesis also requires the formation of a carbanion intermediate, and the presence of an active site base. After α-proton abstraction, the imino acid would be formed parallel to hydride transfer from the substrate α-amino group to the flavin N5 atom (Figure 1b). The third proposed mechanism involves direct hydride transfer of the α-hydrogen of the D-amino acid substrate to the flavin N5 atom, concerted with imino acid formation (Figure 1c). In all cases, the first experimentally detectable reaction intermediate is a charge-transfer complex between the reduced flavin cofactor and the imino acid (the so-called "purple complex" or "purple intermediate"), which dissociates in a step that limits pk-DAAO turnover.

The three-dimensional structures of pig kidney D-amino acid oxidase in complex with various substrate analogues and products have been solved by two independent groups (*23*−*27*), and the structure of the related *Rhodotorula gracilis* enzyme (Rg-DAAO) in the reduced form has been determined at 1.2 Å resolution (*28*). In all cases, no residues properly located to act as the active site base were observed, thus challenging the carbanion mechanism (Figure 1a). Furthermore, the orientation and binding mode of the substrate, with its α-hydrogen pointing toward the flavin N5 position, make electron transfer from the substrate α-amino group to the flavin unlikely (Figure 1b). Indeed, the geometry of the DAAO active site in complex with substrates or substrate analogues is consistent with the "direct-hydride-transfer" mechanism (Figure 1c). The latter is also supported by recent studies using wild-type and mutant forms of mammalian and yeast DAAOs (*29*−*32*).

The DAAO active site geometry does not rule out alternative, although less likely, mechanisms. The α-proton of the amino acid could be transferred to the flavin N5 position, followed by transfer of the electron pair via the formation of a short-lived carbanion intermediate (*30*). However, a radical reaction pattern may be excluded (*19*−*22*) for the first reaction step (eq 1) in DAAO.

With the three-dimensional structures of DAAO at hand, a first-principles molecular modeling study of the enzyme-catalyzed D-amino acid dehydrogenation is feasible and allows, for the first time, mechanistic hypotheses to be tested and provides new insights into the properties of this enzyme.

In the present work extensive ab initio simulations of the pk-DAAO-catalyzed D-amino acid dehydrogenation reaction (eq 1) have been carried out. The large computational requirements of this kind of simulation limit the size of the systems that can be modeled to a few hundred atoms at most, and the time scale of the simulations can hardly extend beyond several picoseconds (*33*). Taking these limitations into account, it has been possible to build a reliable model of the active site of DAAO enzyme with D-alanine as substrate, and to perform a series of "constrained reaction coordinate" simulations (*34*) to study the reactive process. This methodology allowed us to determine the free energy profile for the enzyme reductive half-reaction (eq 1). Furthermore, the structural and electronic transformations brought about by the reaction can be examined in great detail along the reaction path. Therefore, the method provided a microscopic description not only of the minimum (reactant and product) and maximum (transition-state) energy structures, but also of the way in which the transformation gradually takes place between them. The results will be discussed in comparison with the structural and functional experimental evidence available for DAAO.

EXPERIMENTAL PROCEDURES

Car−Parrinello Molecular Dynamics Simulations. All calculations were carried out with the CPMD program (*35*), which performs DFT-based molecular dynamics (MD) simulations within the Car−Parrinello scheme (*3*). The doubly occupied Kohn−Sham orbitals have been expanded in a plane-wave basis set up to an energy cutoff of 60 Ry. Only valence electrons are considered explicitly, and their interaction with the ionic cores was represented by norm-conserving Troullier−Martins (*36*) pseudopotentials. A local pseudopotential was employed for hydrogen, while nonlocal pseudopotentials (in Kleinman−Bylander (*37*) form) including s, p, and d terms represented C, N, and O ionic cores. The gradient-corrected functionals of Becke (*38*) and Perdew (*39*) were employed for the exchange-correlation energy. A time step of 0.121 fs and a fictitious electronic mass of 500 au were used in all the MD simulations.

During building of the enzyme active site−substrate model, the FAD cofactor isoalloxazine nucleus and selected active site protein fragments (see details below) were placed in a periodically repeated cubic supercell, whose edge was chosen about 5 Å larger than the longest interatomic distance measured along each axis. In this way, the system was surrounded by a vacuum region large enough to minimize the interactions with the periodic images in the neighboring cells. The system geometry was optimized, by simulated annealing, with respect to all nuclear degrees of freedom, until the gradients converged to $<5 \times 10^{-4}$ au. At the end of such a process the system was slowly heated to 300 K, all residues (but not the substrate) being held in place by fixing several carbon atoms in positions resulting from the geometry optimization, so as to model the structural effect of the protein framework. All nitrogen, oxygen (except water's), and hydrogen atoms were left free. The C4a and C10a atoms of the FAD molecule, which are expected to undergo important rearrangements in the course of the reaction, were not fixed either. The initial model of the enzyme−substrate complex used for other calculations was determined by repeating the procedure (geometry optimization, heating, and dynamics) on systems comprising an increasing number of active site aminoacyl fragments until a minimal subset of the enzyme active center was found, in which the enzyme−substrate complex appeared to be in a stable conformation. The simulations were carried out on parallel supercomputers, CRAY-T3E (using 64 processors) and IBM-SP3 (using 32 processors), both at CINECA, Bologna, Italy. A single time step took about 50 s in both cases. In the dynamics simulations the temperature is controlled by a Nosé thermostat (*40*) to an average of about 300 K.

Setup of the Model. The atomic coordinates of pk-DAAO in complex with benzoate, a substrate analogue, were used to build the initial model of the oxidized enzyme−D-alanine complex (Protein Data Bank file 1KIF). The enzyme comprises 347 amino acids and one molecule of non-covalently bound FAD. To find a compromise between the size of the system and the resources required to simulate it (*41*), we proceeded by looking for the minimal model adequately describing the enzyme active center.

The three-dimensional structure of the enzyme−benzoate complex (*23*) showed that the DAAO active center can be described as a cavity of 160 Å^3, limited on one side by the isoalloxazine nucleus of FAD and lined mainly by hydrophobic aminoacyl side chains (*23*). The cavity characteristics, such as size, shape, and polarity, are suitable for accommodating small hydrophobic amino acids, DAAO's preferred substrates. A protein loop formed by residues 216−228 provides aminoacyl side chains involved in accommodating and binding the substrate in the active center (Tyr-224 and Tyr-228; *23*, *27*) and forms a lid, which closes the active center and shields it from the bulk solvent. Such an "active site lid" has a role in allowing substrate access and product release, by switching from an "open" conformation to the "closed" structure with the substrate bound to the active site as in the crystal structure (*23*, *27*, *42*). Clearly, any model of the DAAO active site should include the flavin isoalloxazine ring and key residues implicated in substrate binding and should reflect the overall properties of the active site cavity. To identify the minimal requirements of a system reflecting the enzyme−substrate complex, we tested several different models built up by including increasing numbers of residues.

Each model included the FAD isoalloxazine ring cut at the C1′ position of the ribityl side chain and the D-alanine substrate. The latter replaces the benzoate molecule in the X-ray-determined structure (*23*). Initially, the D-alanine substrate was oriented according to the inhibitor-based model of ref *23*, by superimposing the carboxylate groups of the two molecules and the Cα−Cβ bond of D-alanine onto the benzoate C1−C2. The positions of other D-alanine atoms were set to reflect the proper stereochemistry. However, it should be noted that, in all calculations, the positions of D-alanine atoms were left free to detect changes in the substrate position within the DAAO active center model. Fragments of active site aminoacyl residues included in the model(s) were cut from the rest of the protein; their hydrogen atoms, missing in the X-ray structure, were added. Dummy hydrogen atoms were also added to saturate the broken covalent bonds, which connect the residues to the rest of the protein. According to the crystal structures of DAAOs in complex with substrate analogues and products (*23*−*28*), the most important residues involved in substrate binding (Figure 2) are Arg283, Tyr228 (which interact with the substrate α-carboxylate group), and one water molecule (Wat17) whose position is well-defined in pk-DAAO structures (*23*, *25*, *27*). Such "active site water" is held in place through formation of hydrogen bonds with Gln53 and Gly313 main chain carbonyl oxygens and with the Tyr224 side chain hydroxyl group. Therefore, the first model we tested included fragments corresponding to Arg283, Tyr228, Gln53, and Gly313. D-Alanine was introduced as the anion $NH_2CH(CH_3)COO^-$ to balance the positive charge on the Arg283 guanidinium fragment and to maintain the overall neutrality of the system. Indeed, the simulation of isolated charged systems is computationally much more demanding than the simulation of neutral systems (*43*). However, the assumption is justified in the case of D-amino acid oxidase since kinetic studies have shown that the substrate α-amino group must be unprotonated for catalysis (*31*) so that a proton must be lost from the charged amino group upon binding to the enzyme active site. Therefore, in our simulations we are looking at a situation in which such a deprotonation step has already taken place. We have not tested here the

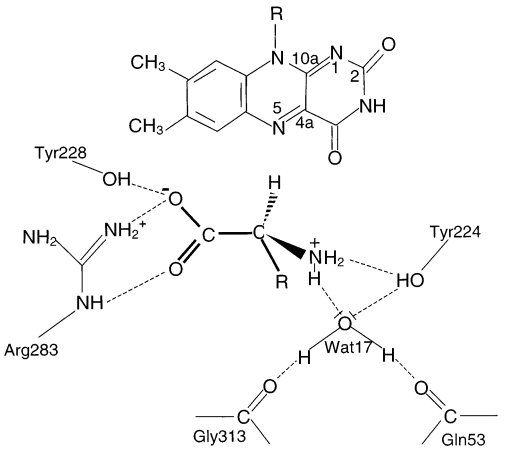

FIGURE 2: Schematic representation of the DAAO active site and of the essential interactions between the protein aminoacyl residues and the D-amino acid substrate. The scheme was drawn from ref *19* by modeling the D-alanine substrate on the basis of the benzoate position in the experimentally determined (*19*) enzyme−benzoate complex structure by superposing the D-alanine and benzoate carboxylate groups and D-alanine Cα−C*β* bond and benzoate C1−C2 bond. Bonds used for such superposition are in bold. Numbering of the relevant positions of the FAD isoalloxazine ring is also indicated.

possibility that binding of D-alanine in the zwitterionic form could lead to its positioning with the α-amino group pointing toward the flavin N5, as in Figure 1b: on the basis of steric factors, this would require a major rearrangement of the active center residues. This rearrangement was not observed with any of the experimentally determined DAAO crystal structures (*23*−*28*).

With this and other models of increasing complexity, we carried out geometry optimization, heating, and dynamics calculations as described above, but we observed that, already in the heating phase, the substrate quickly left the active site model, indicating that the model was not adequate to describe the pk-DAAO active center. Therefore, we proceeded by adding other fragments, and by repeating the above procedure (geometry optimization, heating, and dynamics) until we found a stable configuration, i.e., a model able to bind the substrate and hold it in place. At difference with the previous, incomplete models, D-alanine showed only oscillations in the active site, and no repositioning occurred after 3 ps of unconstrained dynamics, while in the other cases the substrate was clearly seen to move away after 200−300 fs. Moreover, the average force of constraint calculated for this model (see below) was close to zero, indicating that D-alanine is indeed in a stable equilibrium configuration.

Such a final model consists of 141 atoms (11 aminoacyl fragments plus the flavin isoalloxazine nucleus and the D-alanine substrate) enclosed in a cubic box with a side of 19.42 Å. The optimized geometry is shown in Figure 3a, where the X-ray-crystallography-determined structure of pk-DAAO has been superimposed.

The fragments included in the final enzyme−substrate model were (clockwise from the top of Figure 3a) the alkyl side chains of Leu51, Ile230, and Ile215, the polar part of the phenol ring (as a $CH_2{=}C(CH_3)OH$ moiety) of Tyr228, the positive $[CH_3{-}NH{-}C(NH_2)_2]^+$ guanidinium fragment of Arg283, the peptide bond between Gly313 and Tyr314 as a $CH_3{-}NH{-}CO{-}CH_3$ moiety, the peptide bond between residues Pro54 and Gln53 as a $CH_3{-}NH{-}CO{-}CH_2{-}NH{-}CH_3$ moiety corresponding to the main chain atoms and with the last methyl replacing the Trp52 carbonyl, and Tyr224 as a $CH_2{=}CHOH$ group, as done for Tyr228 but without the methyl group.

After the heating phase, a trajectory of 2 ps at 300 K was carried out: the (unconstrained) D-alanine molecule showed only librations and vibrations, but did not translate outside nor rotate inside the model active site cavity, roughly maintaining the same orientation as in the optimized structure (Figure 3a) and as predicted by the 70 K X-ray structures (*23*−*28*). The stability of the substrate in the final model (and presumably in the real enzyme) seems to arise from two concurring effects: the strong attractive interaction between the D-alanine carboxylate and the positive guanidinium fragment of Arg283 (see below) is essential to hinder substrate rotation and translation, but only when combined with the additional steric interaction, with all the additional fragments completing the cavity walls. Indeed, in the absence of the latter interactions the substrate moved away from the active site immediately after the dynamics simulation was started.

The good match between the energy-minimized structures of the enzyme−substrate complex calculated by us at 300 K and that determined by X-ray crystallography at 70 K (Figure 3a) is relevant to validate both techniques. Indeed, protein diffraction studies are carried out at very low temperature, while our ab initio molecular dynamics simulation is run at 300 K, even if for a short elapsed time. Computer minima are found that are very similar to low-temperature X-ray-determined structures, and on the other hand, Car−Parrinello simulations show that low-temperature X-ray structures do not differ substantially from room-temperature behavior of the substrate inside the enzyme cage.

Controlling the Reaction: Sampling the Blue Moon Ensemble. The rate constant for flavin reduction (eq 1) has been directly measured by stopped-flow spectrophotometry to be in the 1225−4000 s^{-1} range (*29*, *44*), corresponding to an activation energy of 12.6−13.3 kcal/mol, at 25 °C. The crossing of this energy barrier is a *rare event* on the time scale of typical microscopic simulations, and special techniques are required to enhance the sampling of the low-probability region near the barrier top. The blue moon ensemble method of constrained molecular dynamics (*34*, *45*) allows a particular reaction path to be sampled and the corresponding free energy profile as a function of a chosen reaction coordinate, q, to be obtained. The reaction coordinate is initially assigned a value of q_R corresponding to the reactants, and a simulation is performed with the constraint $q = q_R$. Then a series of finite-temperature dynamics simulations are performed, varying the q value in small steps from q_R to a value of q_P typical of products. In each simulation the constraint force needed to keep the constraint at the imposed value is calculated and averaged until its mean value shows no more drift. By integrating the mean force $\langle F(q)\rangle$ along the reaction path, the change in free energy between two points, A and B, can be computed according to eq 4.

$$\Delta G = -\int_{q_A}^{q_B} \langle F(q)\rangle \, dq \qquad (4)$$

This method allows estimation of the free energy profile of

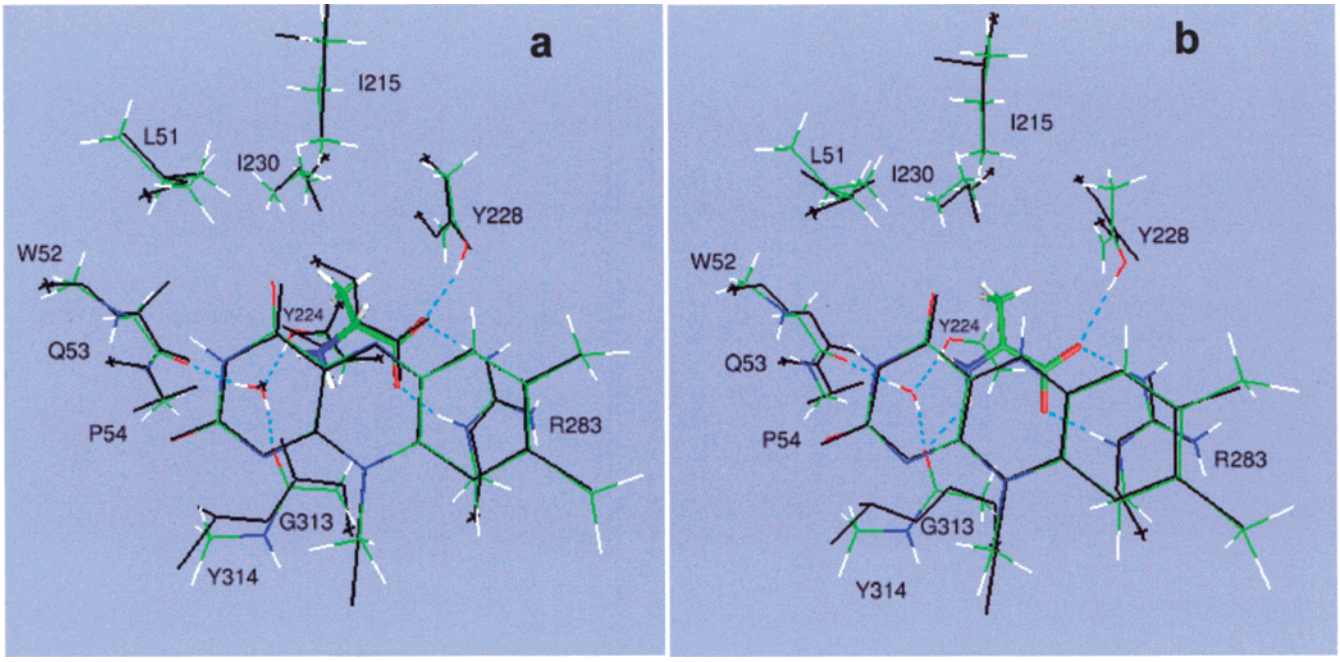

FIGURE 3: Optimized model geometries of the oxidized flavin−D-alanine (a) and reduced flavin−iminopyruvate (b) complexes. The corresponding experimentally determined structures (PDB accession codes 1KIF and 1DD0, respectively) have been superimposed as black sticks, with ×'s indicating the points where covalent bonds have been cut. The superimposition has been performed in such a way to achieve the best overlap between the modeled and experimental FAD units and by rotating the rest of the system accordingly. Atom color key: H, white; C, green; N, blue; O, red.

the reaction. Interestingly, no prior knowledge of the transition-state structure or of its corresponding reaction coordinate value is needed. On the contrary, the system is smoothly led from the reactants to the products, exploring the configurations available at a finite temperature, thus following a reliable and accurate reaction path. However, the choice made about the relevant reaction coordinate controlling the course of the reaction is essential for the success of the method. To model substrate dehydrogenation catalyzed by DAAO, we decided to use the transfer reaction coordinate (*5*) defined as

$$q = R_{CH} - R_{NH} \tag{5}$$

where R_{CH} is the distance between the proton and the Cα carbon of D-alanine and R_{NH} is the distance between the same proton and the flavin N5 atom. On the reactant side q is negative, while it changes sign on the product side. However, as the reaction may not be symmetrical, the transition state is not necessarily located at $q = 0$. Indeed, the zero value of the mean constraint force is actually used to identify the transition state (*5*). Compared to constraining a single distance or angle, the present choice for q is more flexible in that it avoids any direct restriction on the Cα−N5 distance, as well as on the Cα−H−N5 angle: both values can vary following the course of the reaction. The initial value for q was fixed to −1.32 Å, taking the last value of q from the trajectory performed with the oxidized enzyme−substrate model (Figure 3a) without constraints. Then a 4 ps constrained trajectory was carried out, and the mean constraint force averaged over the last 3 ps. The bias on the phase space averages introduced by the constraint must be taken into account by an appropriate reweighing of the quantity to be averaged. In the case of mean force, the Lagrange multiplier associated with the force of constraint for the present reaction coordinate was properly reweighed according to ref *45*. The mean force converged to its final value within the first picosecond; therefore, the next constrained trajectories were extended for 1.5 ps at most, always checking for the convergence of the mean force. The final configuration of each constrained trajectory was taken as the starting point of the next one, with the distances involved in the reaction coordinate adjusted to increase q by ∼0.25 Å at a time.

A clear description of the electron distribution along bonds and atoms has been obtained at several points for each constrained simulation via a Wannier transformation of the Kohn−Sham eigenfunctions (*46*), giving localized orbitals (analogous to the Boys orbitals; *47*), which minimize the spread for each electronic state. In particular, the plot of the centroids of the Wannier functions (WFCs) at each point along the reaction path provides a dynamic view of the electronic displacements and rearrangements during the reaction (*48*).

RESULTS AND DISCUSSION

Free Energy Profile of the DAAO-Catalyzed D-*Alanine Dehydrogenation Reaction.* Ten constrained trajectories have been carried out, and the mean constraint force as well as the free energy profile were calculated according to eq 4, and are reported in Figure 4. A negative constraint force implies that the proton is pulled toward the D-alanine α-carbon. On the contrary, when the force is positive, the proton is pulled toward the flavin N5 atom. The mean force should be zero at the extrema along the reaction path: reactant, transition state (TS), and products. The TS is located at $q = 0.25$ Å. At this point, the free energy profile reaches a maximum and the mean force value is zero (Figure 4). Due to the asymmetry of the reaction, the trend from the TS to the products does not mirror the trend on the reactant side. Indeed, when $q \approx 1.3$ Å, the mean force is still far from

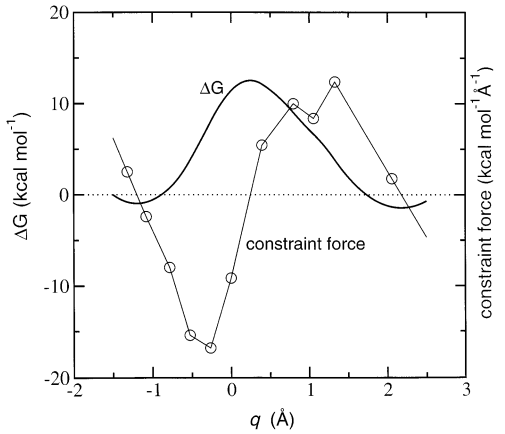

FIGURE 4: Energetics of the modeled DAAO-catalyzed D-alanine dehydrogenation reaction. Mean constraint force (thin line) and free energy (thick line) values calculated as a function of the reaction coordinate *q*.

zero. To locate the *q* value corresponding to the products, the constraint on the reaction coordinate was released starting from the last configuration with $q \approx 1.3$ Å, and leaving the reaction product (2-iminopyruvate) free to settle in the active site without constraints. With such constraints removed, the substrate slightly moved away from the now reduced flavin without changing its orientation, until the difference $R_{CH} - R_{NH}$ reached a stable value of approximately 2 Å. The latter value was taken as the reaction coordinate value for the reaction product in complex with the reduced enzyme. A further constrained trajectory with $q = 2$ Å was performed to ensure that the product energy well was reached. Indeed, the mean force calculated with this constraint converged to a value close to zero (Figure 4). On the basis of the free energy profile (Figure 4), the activation free energy for the reaction was 13.305 kcal/mol. This value must be compared with the experimentally determined values of 12.6−13.3 kcal/mol (*29*−*44*). The excellent agreement between the calculated and observed values of the activation energy of the DAAO reaction supports the conclusion that the model and the calculations provide an accurate description of the reaction under study.

At this point, with both a good starting configuration as compared with the experimentally determined X-ray structure and good agreement with kinetic results, we are in a position to discuss the microscopic details of the reaction mechanism for the enzyme-catalyzed dehydrogenation of D-alanine (eq 1).

Structures of the Oxidized DAAO−D-*Alanine and Reduced DAAO*−*Iminopyruvate Model Systems*. To compare the structural features of our model with those of the enzyme in complex with substrate analogues determined by X-ray crystallography (*23*−*25*), the optimized geometry of the reactants (see above) has been superimposed onto the corresponding residues in the X-ray structure of ref *23* (Figure 3a). Most of the residues included in our model to mimic DAAO active site functional groups keep rather close to their starting (crystallographic) positions. The small rearrangements shown, e.g., by Gly313−Tyr314 fragments, can be ascribed to the incomplete protein structure of the model, which allows for the observed conformational differences between the model and the enzyme crystal structure. However, the calculated geometry is within the resolution of the X-ray experiments. Despite the fact that none of the D-alanine atoms were fixed during the calculations, the D-alanine substrate keeps the initial orientation with its α-hydrogen pointing toward the flavin, and with the Cα−N5 distance of 3.38 Å, very close to the value of 3.4 Å calculated from the DAAO crystal structure (*23*). The substrate is held in place by the double hydrogen bond between its carboxylate group and the guanidinium group of Arg283. The hydroxyl group of Tyr228 is also H-bonded to the amino acid α-carboxylate. These interactions reproduce those inferred from the analysis of the structure of DAAO in complex with the substrate analogues benzoate (*23*, *24*) and *o*-aminobenzoate (*25*). The same is true for the hydrogen bonds involving the active site water molecule, which interacts with the hydroxyl group of Tyr224 and with the carbonyl groups of Gly313 and Gln53. At variance with the model based on the crystallographic structure of the DAAO−benzoate complex (*23*), our optimized structure does not show H-bonds involving the amino group of the substrate. Such a difference can be ascribed to the fact that in our model the substrate α-amino group is neutral, while in the model of ref *23* (see Figure 2) it is positively charged. However, the overall similar geometries of the crystallographic and computed enzyme−substrate complexes demonstrate that protonation of the substrate α-amino group does not influence the orientation of the D-alanine substrate in the enzyme active center. Furthermore, the crystallographically and computationally determined geometries both contribute to rule out mechanism 1b as a likely reaction mechanism for D-alanine dehydrogenation reaction catalyzed by DAAO.

At the end of the reaction, we optimized the geometry of the reduced enzyme−iminopyruvate product complex. The minimum energy structure has been superimposed (Figure 3b) onto the experimental structure of reduced pk-DAAO in complex with the reaction product α-iminotryptophan (iTrp; *27*). In the latter structure the bulky iTrp side chain appears to have induced a considerable rotation of Tyr224 to accommodate it and, as a likely consequence, to have displaced the active site water molecule (*23*−*27*). These modifications are not expected to occur with the smaller D-alanine substrate. Thus, Tyr224 has been omitted for clarity from the experimental structure in Figure 3b. Indeed, in the crystal structures of the reduced DAAO−Δ^1-pyrrolidine-2-carboxylate (DPC; *26*) and of the covalent DAAO−ketovaleric acid complex (*27*), the active site water molecule and the residues keeping it in place in the active center through H-bond interactions (namely, Gln53 and Gly313 carbonyl oxygens and the Tyr224 hydroxyl group) are found in positions indistinguishable from those observed in the DAAO−benzoate complex. Furthermore, such active site water and its interacting residues are present also in the X-ray structure of the reduced Rg-DAAO in complex with D-alanine (*28*).

Overall, the positions of the residues in our optimized structure do not show large deviations from the corresponding crystallographic positions. The same hydrogen bond network as that observed for the oxidized enzyme−D-alanine complex is observed, with an additional H-bond between the (now positive) NH_2 group of the imino acid product and Gly313 carbonyl oxygen. Interestingly, a similar H-bond between the product iminium ion and Gly313 carbonyl oxygen is observed in the reduced DAAO−iTrp complex

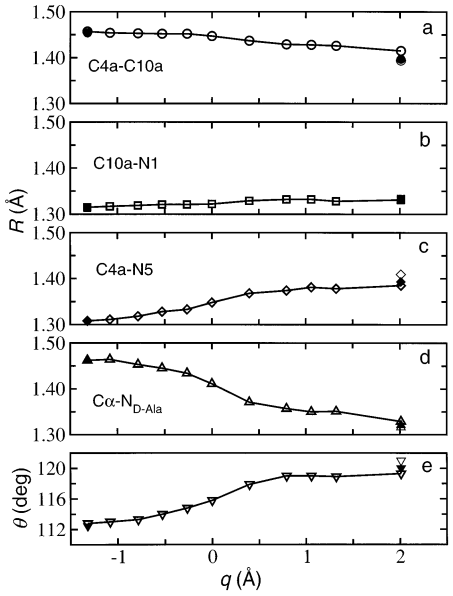

FIGURE 5: Evolution of characteristic distances and angles along the reaction path: (a−d) the distances *R* between the atoms indicated have been calculated as time averages along each constrained trajectory; (e) θ, the mean value of the three relevant angles about Cα ($H_2N-C\alpha-CH_3$, $H_2N-C\alpha-COO^-$, and $CH_3-C\alpha-COO^-$), averaged during the course of the reaction as the previous distances; empty symbols, time averages; full symbols, optimized geometries; gray symbols, geometry of the products with the dipole added (see the text for details).

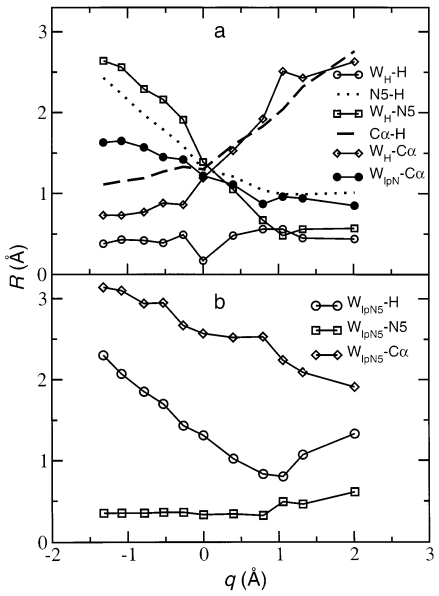

FIGURE 6: Evolution of the main distances *R* between characteristic WFCs and atomic centers. (a) Distances between the indicated atoms and WFCs originally on the substrate: W_H, WFC originally belonging to the Cα−H bond; W_{lpN}, lone pair amino nitrogen WFC. The interatomic N5−H (dotted line) and Cα−H (dashed line) distances are also reported for comparison. (b) Distances between the indicated atoms and the N5 lone pair WFC. See Figure 8 for the identification of WFCs.

(although in the absence of the active site water molecule; *27*) and in the reduced DAAO−DPC complex (*26*). This additional interaction could play an important role in stabilizing the reaction products. Finally, in both the oxidized and reduced forms the flavin ring in the optimized structures is essentially planar, also in good agreement with the experimentally determined structures (*23*−*28*). However, in the MD simulations the thermal motions induce small distortions from planarity, which are more marked for the reduced flavin. The overall good agreement between the minimum energy geometries of our model and the corresponding X-ray structures shows the reliability of the computational method and, in particular, of the approximations made in model building, namely, the exchange-correlation density functional chosen, or the limited size of the system and the use of a periodic supercell to represent it.

Analysis of the Reaction Path. Figure 5 shows the variation of several relevant distances and angles during the reaction; the reported values have been averaged over each constrained trajectory. They provide a clear picture of the structural modifications taking place in the course of the reaction. The expected electron shift (Figure 1) when the flavin is reduced by two electrons on the N5 atom involves the reduction of the C4a−N5 and C10a−N1 bond order and the shortening of the C4a−C10a bond. The evolution of the C4a−C10a (Figure 5a), C10a−N1 (Figure 5b), and C4a−N5 (Figure 5c) distances is generally consistent with this electron rearrangement, albeit the increase in the C4a−N5 distance is more marked than the variations of the C4a−C10a and, particularly, C10a−N1 distances. This point indicates that the electron density shifted away from the N5−C4a region does not completely move to the N1 position as depicted in Figure 1. Rather it extends to other regions of the isoalloxazine moiety as we will discuss in greater detail in the following sections.

The bond length modifications occur in a continuous process as soon as the α-proton moves away from the substrate toward the flavin N5 atom. Such a process parallels the changes observed for the D-alanine Cα−N bond length (Figure 5d) and θ (average of $H_2N-C\alpha-CH_3$, $H_2N-C\alpha-COO^-$, and $CH_3-C\alpha-COO^-$ angles) in Figure 5e. The formation of a planar imino acid, with a shorter C−N distance than in the tetrahedral D-alanine substrate, is evident. The most important point is that this transformation occurs smoothly and simultaneously as the reaction proceeds. This observation constitutes the first evidence of a *concerted* mechanism: indeed, if a carbanion intermediate was formed during the reaction, the initial tetrahedral angle and C−N single bond characters of the substrate would have been conserved at least for a part of the reaction path, giving rise to horizontal segments in panels d and e of Figure 5. Therefore, the electron transfer occurs *in parallel with the transfer of the hydrogen atom*. Taken together such observations lead to the conclusion that our model represents the first reaction step (eq 1) according to a concerted hydride-transfer mechanism in which formation of the iminium ion takes place at the same time as a hydride ion is transferred from the amino acid substrate to the flavin redox center. The fact that the calculated activation barrier *for this hydride transfer* coincides with the experimental measure for the reaction step in eq 1 supports the conclusion that the enzyme-catalyzed reaction proceeds by a hydride-transfer mechanism.

Electronic Distributions along the Reaction. A picture of the electronic structure evolution can be obtained by inspecting the WFC position and spatial dispersion (σ) as the reaction proceeds (*48*) (Figures 6 and 7). For each *q* value, the figures show the WFCs calculated for the final config-

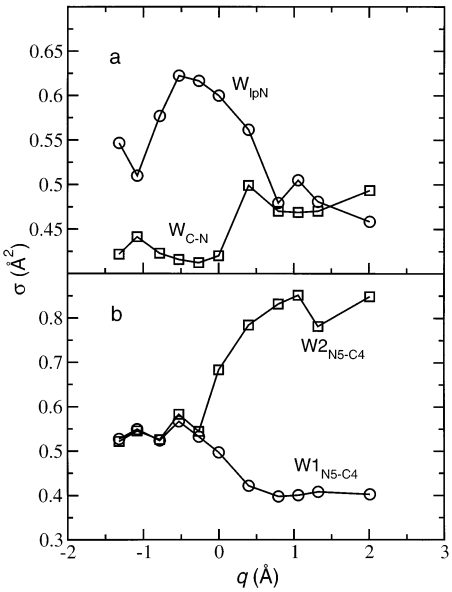

FIGURE 7: Spatial dispersion (σ) of the main WFCs along the reaction path: (a) WFCs belonging to the substrate; (b) WFCs originally on the N5−C4a double bond; W_{lpN}, lone pair amino nitrogen WFC; W_{C-N}, WFC originally on the Cα−N bond; $W1_{N5-C4}$ and $W2_{N5-C4}$, WFCs originally on the flavin N5−C4a double bond. See Figure 8 for the identification of WFCs.

uration of the corresponding constrained trajectory. In our calculation scheme with doubly occupied orbitals, each WFC position corresponds to the center of charge density of the maximally localized orbital describing an electron pair, while its spatial dispersion is proportional to the delocalization extent of the orbital.

Note that the two Wannier centers involved in a double bond are symmetrically located on both sides of the bond axis, while the WFC of an ordinary single bond is located exactly on the bond axis. Moreover, an electron pair involved in a single bond becomes less localized when a double bond is formed; thus, its spatial dispersion increases, as it also does for instance when it is involved in charge-transfer processes (*48*).

We considered the WFCs originally belonging (i.e., closest) to the substrate Cα−H bond (W_H), to the Cα−N bond (W_{C-N}), and to the initial lone pairs on the D-alanine amino nitrogen (W_{lpN}) and on N5 (W_{lpN5}) and the WFCs originally involved on the flavin N5−C4a double bond ($W1_{N5-C4}$ and $W2_{N5-C4}$) and on the N1−C10a double bond ($W1_{N1-C10}$ and $W2_{N1-C10}$, Figure 8a); their initial/final positions are shown in Figure 8b,c.

As shown in Figure 6a, W_H closely follows the transferred proton (open circles), leaving Cα (open tilted squares), and approaching N5 (open squares); this confirms that the transferred species is a hydride ion, with a minimum W_H−H distance of 0.17 Å when the R_{CH} and R_{NH} distances are equal ($q = 0$). The N5−H bond is formed when $q > 1$ Å. On the substrate side, while the proton is being transferred to the flavin, the WFCs on D-alanine rearrange with two electron pairs in the C−N interatomic region. Figures 6a (full circles) and 8b highlight the formation of the imino acid Cα−NH_2 double bond with the displacement of W_{lpN} in the C−N region closer to the α-carbon. The convergence of the σ values of W_{C-N} and W_{lpN} (Figure 7a) supports this observation. The trend of the curves in Figure 6a supports the previous conclusion that the imino acid is gradually formed in a concerted way as the hydride ion is transferred. These results are in excellent agreement with conclusions drawn from the observations of kinetic nitrogen isotope effects with pk-DAAO (*31*) and of structure/linear free energy correlations and deuterium kinetic isotope effects using substituted phenylglycines and *Trigonopsis variabilis* DAAO (Tv-DAAO; *30*).

Structure and Electronic Distribution of the DAAO-Bound Reduced Flavin Isoalloxazine Moiety. The analysis of the electronic distribution on the flavin ring also provides insight into the DAAO-catalyzed reaction. As the transferred hydride ion comes within bonding distance with respect to the flavin N5 atom, we observe a significant rearrangement of the internal electronic distribution over the flavin isoalloxazine ring. As noted before, from the mechanism of Figure 1 a substantial change in the electronic distribution is expected to take place in the N5−C4a−C10a−N1 region of the isoalloxazine ring. Contrary to these expectations, in our model such developing negative charge does not appear to be localized on the N1 atom nor on the whole pyrimidine ring. Rather, the presence of a WFC close to the C4a atom, which was absent in the oxidized flavin (compare the position of $W2_{N5-C4}$ (center 5b) in Figure 8b,c), suggests charge localization on this atom. The second pair ($W1_{N5-C4}$, center 5a) is shifted on the C4a−N5 bond axis, to form a single bond (Figure 8c). The dispersions associated with these centers, reported in Figure 7b, are consistent with these transformations. The final position of $W2_{N5-C4}$ is out of the flavin plane, in the region between FAD and the imino acid (Figure 8c). On the other hand, the W_{N1-C10} electron pairs (centers labeled as 6 in Figure 8) show only a negligible displacement toward N1 in the reduced flavin.

An increase of electron density at C4a has been observed by ^{13}C NMR spectroscopy (*49*) in the charge-transfer (CT) complex between anionic reduced flavin and zwitterionic imino acid (the DAAO purple complex; see below). Furthermore, the electron density distribution on reduced flavin in the reduced Rg-DAAO−D-alanine complex (*28*) is also consistent with our result. The localization of electron density on the flavin C4a position, as opposed to charge delocalization over the pyrimidine ring or the N1−C(2)═O position has been proposed to be relevant in the ability of DAAO-bound flavin to react with molecular oxygen in the second partial reaction (eq 2; *19*−*22*). It is generally accepted that in the reoxidation of flavin by molecular oxygen (eq 2) electrons are transferred (most likely in a stepwise process) from C4a to O_2. Therefore, the ability of the enzyme active site residues to maintain/concentrate a high electron density on C4a contributes to catalysis of the oxygen reduction reaction.

In addition, it has been suggested that the formation of the stable CT complex plays an essential role in maintaining a high charge density on the C4a position (*26*). Our calculations provide evidence of a weak charge transfer from the reduced flavin to the charged α-imino acid. The evolution of W_{lpN5} distances in Figure 6b shows that after the formation of the N5−H bond ($q > 1$ Å) the electronic distribution near N5 is polarized toward the oxidized substrate. Moreover, $W2_{N5-C4}$'s dispersion remains significantly large even after product formation (Figure 7b). These observations suggest that there is indeed some charge transfer from the reduced

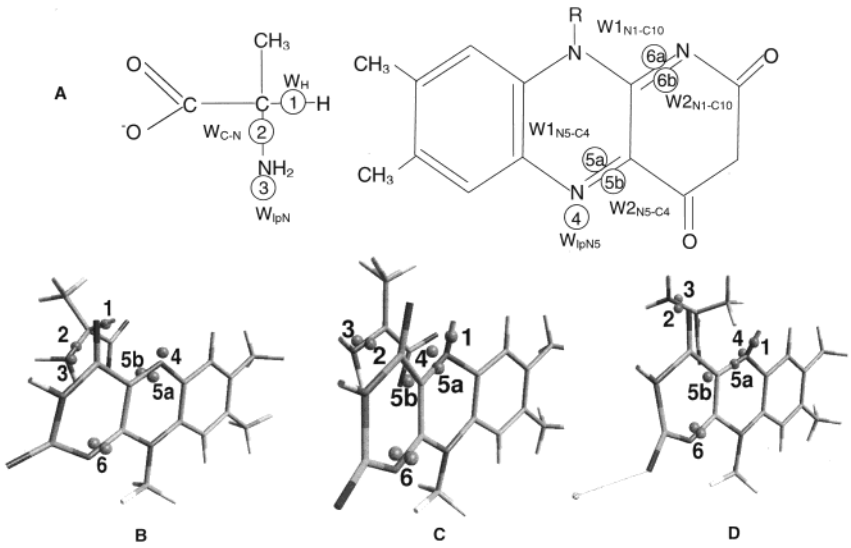

FIGURE 8: Identification of relevant WFCs. (A) Labeling of relevant WFCs: 1, W_H; 2, W_{C-N}; 3, W_{lpN}; 4, W_{lpN5}; 5a, $W1_{N5-C4}$; 5b, $W2_{N5-C4}$; 6a and 6b (later marked as 6), $W1_{N1-C10}$ and $W2_{N1-C10}$, respectively. (B−D) Position of selected WFCs in the enzyme−substrate model complex (B), in a configuration taken from the last trajectory with the "free products" (C), and in a configuration taken from the last trajectory with the free products after inclusion of the dipole, whose hydrogen atom H-bonded to O2 is shown in the lower left corner (D).

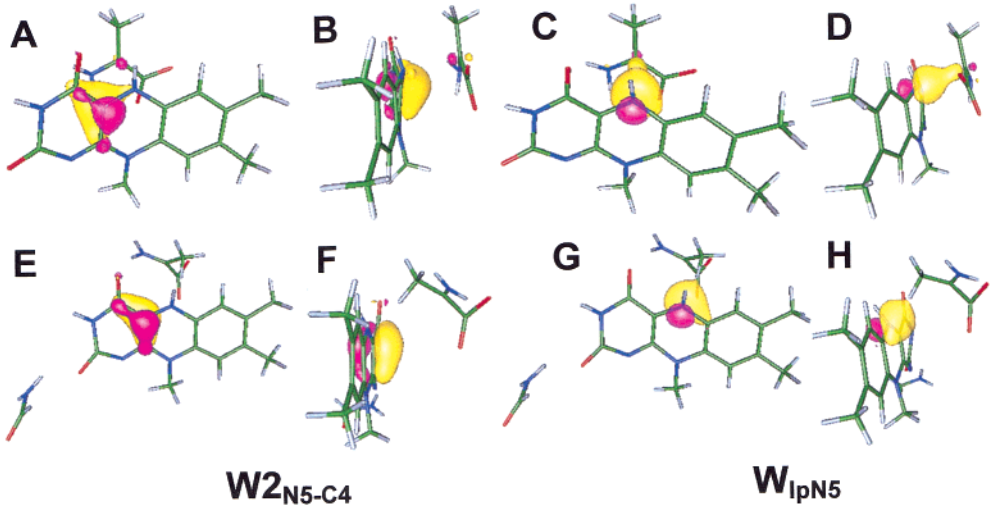

FIGURE 9: Wannier orbitals occupied by the two electron pairs involved in the DAAO−iminopyruvate charge-transfer interaction. Top row: $W2_{N5-C4}$ (A, B) and W_{lpN5} (C, D) in the DAAO−iminopyruvate CT complex. Bottom row: $W2_{N5-C4}$ (E, F) and W_{lpN5} (G, H) in the DAAO−iminopyruvate CT complex including the dipole (shown in the lower left corner of panels E and G). Positive and negative isosurfaces are shown in yellow and purple, respectively.

flavin (both from C4a and N5) to the imino acid when they are close together.

To confirm and clarify the nature of this effect, the two Wannier orbitals having $W2_{N5-C4}$ and W_{lpN5} centroids are shown in Figure 9 (top). The first one is indeed centered on C4a (Figure 9A,B). It spreads over C1, N5, and C10a on both sides of the flavin plane, with a larger lobe in the region toward the imino acid. The orbital occupied by the N5 lone pair (Figure 9C,D) is less delocalized in the flavin plane but shows a considerable charge density along the N5−Cα axis. Therefore, it appears that the CT complex arises from the shift of electronic charge both from C4a and, to a greater extent, from N5 toward the imino acid, in agreement with NMR experiments (*49*) showing an electron-rich C4a in the purple complex.

Role of the αF5 Helix Dipole. To further investigate these points, e.g., to establish whether the charge localization on the reduced flavin C4a position could effectively be triggered by the CT interaction with the imino acid, we performed a further geometry optimization and MD trajectory after inserting into the simulation box a $HCONH_2$ molecule where the pk-DAAO Leu316−Thr317 peptide bond is located. Indeed, it is reported that the large dipole of helix αF5 (whose positive end is close to Thr317) could play a key role in the stabilization of the negative charge of the reduced anionic flavin on the N1−C2═O2 locus (*19*−*23*). Due to limits imposed by both the size of our model and the difficulty to evaluate the precise value of the helix dipole (which may be influenced by surrounding protein residues), we tried to mimic its effect by positioning a local dipole directed with its positive end toward O2. After reoptimizing the geometry of the reduced enzyme−imino acid complex, we found small rearrangements in the distances of key atoms as reported in Figure 5 (gray symbols). More relevant to the present discussion is the fact that *the inclusion of the dipole has the effect of destabilizing the CT complex*. In fact, we

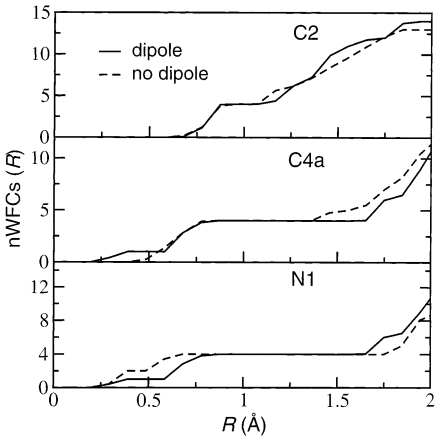

FIGURE 10: Cumulative numbers of WFCs contained in a sphere of radius *R* centered on the flavin C2, C4a, and N1 positions in the presence (continuous line) and in the absence (dashed line) of the dipole adjacent to the N(1)−C(2)═O position of the reduced flavin.

performed an MD simulation of the reduced flavin−imino acid−dipole system without constraints on the reaction coordinate. In this system, the imino acid left free appears to be more mobile than in the system without the dipole. After 0.1−0.5 ps it considerably rotates and changes orientation, pointing its methyl group toward the flavin ring (Figure 8d). The larger mobility of the imino acid in the model containing the dipole could be related to the "pulling" (electron-withdrawing) effect of the dipole positive end. This reduces the polarization of the electronic charge toward the imino acid, with the consequence that the CT interaction between the reduced flavin and the imino acid product discussed above is disrupted. The disappearance of the CT complex can be deduced first by looking at Figure 8d, where the relevant WFC positions when the dipole is present are shown. After the inclusion of the dipole and the rotation of the imino acid, the displacement of the W_{lpN5} and $W2_{N5-C4}$ centers toward the imino acid is reduced. The corresponding Wannier orbitals are shown in Figure 9E−H. The $W2_{N5-C4}$ orbital shows only minor changes (note however the disappearance of the two small lobes on Cα with respect to Figure 9A−D); a greater change is observed for the W_{lpN5} orbital, where the considerable shift of charge toward the imino acid disappears. This confirms that the CT interaction mainly took place from the N5 lone pair.

The CT complex thus appears to be labile in our model, and its stability is strongly affected by long-range effects, as the electrostatic effect of the dipole. It is worth pointing out that the DAAO purple complex is a stable intermediate in the reaction of pk-DAAO with D-alanine, and this is typical of DAAO from pig kidney. In the other well-characterized DAAOs, namely, Rg-DAAO and Tv-DAAO, such a charge-transfer complex does not build up due to a greater dissociation rate as compared to that observed in the pig kidney enzyme (*50*). Such a different stability of the purple intermediate correlates with the presence in pk-DAAO (*23*), but not in Rg-DAAO (*28*), of the 216−228 active site lid, which is missing in our present model as well. The poor stability of the purple complex we observe supports the hypothesis of the role of the enzyme active site lid in controlling substrate/product binding to the enzyme active site (*27*, *42*).

Another interesting point is that the loss of the CT complex determines only a slight decrease of the charge localization on the flavin C4a atom; this was already implicit when we emphasized its minor importance in the CT interaction. A small shift of electronic density from the C4a toward N1−C2═O2 can be highlighted by calculating the number of WFCs close to N1, C2, and C4a (Figure 10). The presence of the dipole has the effect to shift almost two WFCs closer (within 2 Å) to N1 and C2, at the expense of WFCs close to C4a. However, the charge remains centered mainly on C4a even in the absence of the CT complex (Figure 8d), indicating that, at variance with the previous conclusion (*26*), it is *not the presence of the positive end of the zwitterionic imino acid in the CT complex that determines and stabilizes the charge accumulation on the flavin C4a position*.

CONCLUSIONS

We have shown here that modeling of the active center of DAAO is feasible, and that a reliable description of the enzyme-catalyzed D-alanine dehydrogenation can be obtained to complement information obtained by kinetic and equilibrium studies in solution and by X-ray crystallography. The present computational approach led to the conclusion that the crystallography-based models of the enzyme−substrate and enzyme−product complexes reflect stable conformations of the system.

The transfer of the substrate α-hydrogen to the flavin N5 position has been simulated, and the free energy profile of the reaction and the electronic distributions are consistent with the proposal that the DAAO-catalyzed reaction proceeds by a hydride-transfer mechanism, which is tightly coupled to imino acid formation (Figure 1c). Thus, the alternative (and unlikely) mechanism (see ref *26* for a discussion) which implies transient formation of a carbanion intermediate with the flavin N5 position acting as the proton acceptor is also not supported by the present data. A weak reduced flavin−imino acid charge-transfer complex is observed in our model, and such a CT complex is further destabilized by the presence of a dipole near the flavin N1−C2═O locus. The poor stability of the reduced enzyme−imino acid CT complex highlights a role of the DAAO active site lid in stabilizing such reaction intermediate. In contrast with earlier proposals, charge transfer to the imino acid in the purple complex originates from the N5 lone pair rather than from C4a. Furthermore, regardless of the presence of the dipole and of the presence of the charge-transfer interaction between reduced flavin and the iminopyruvate product, electron density remains localized around the C4a position of the two-electron-reduced flavin, thus priming the reaction of the reduced enzyme with molecular oxygen.

Contrary to expectations, the positive end of the αF5 helix dipole does not appear to be necessary to enhance flavin reactivity in the D-alanine dehydrogenation reaction nor to affect to any significant extent the electron density distribution on the flavin isoalloxazine ring. The activation energy for the reaction calculated in the absence of the dipole closely matches that determined experimentally in solution studies: this could indicate that the dipole is not essential for catalysis of D-alanine dehydrogenation. Rather, we have found that it plays a role in destabilizing the DAAO purple intermediate through a mild electron-withdrawing effect that subtracts

charge density from the C4a−N5 region. This reflects the importance of long-range effects in controlling product stability.

The extension of the present approach to obtain mechanistic information on other flavin-dependent enzymes appears possible. Furthermore, the application of this approach to the study of the reaction of reduced DAAO with molecular oxygen, which has escaped experimental investigations, would be particularly interesting.

ACKNOWLEDGMENT

Prof. B. Curti and A. Mattevi are thanked for helpful discussions during the course of this work.

REFERENCES

1. Allen, M. P., and Tildesley, D. J. (1987) *Computer Simulations of Liquids*, Clarendon Press, Oxford.
2. Frenkel, D., and Smit, B. (1996) *Understanding Molecular Simulations*, Academic Press, New York.
3. Car, R., and Parrinello, M. (1985) *Phys. Rev. Lett. 60*, 2471.
4. Curioni, A., Sprik, M., Andreoni, W., Schiffer, H., Hutter, J., and Parrinello, M. (1997) *J. Am. Chem. Soc. 119*, 7218.
5. Meijer, E. J., and Sprik, M. (1998) *J. Am. Chem. Soc. 120*, 6345.
6. Raugei, S., and Klein, M. L. (2001) *J. Phys. Chem. B. 105*, 8212.
7. Fois, E., Gamba, A., and Tabacchi, G. (2000) *Chem. Phys. Lett. 329*, 1.
8. Carloni, P., Sprik M., and Andreoni, W. (2000) *J. Phys. Chem. B 104*, 823.
9. Piana, S., and Carloni, P. (2000) *Proteins: Str. Func. Gen. 39*, 26.
10. Röthlisberger, U., and Carloni, P. (1999) *Int. J. Quantum Chem. 73*, 209.
11. Piana, S., Sebastiani, D.; Carloni, P., and Parrinello, M. (2001) *J. Am. Chem. Soc. 123*, 8730.
12. Alber, F., and Carloni, P. (2000) *Protein Sci. 9*, 2535.
13. Hohenberg, P., and Kohn, W. (1964) *Phys. Rev. 136*, B864.
14. Kohn, W., and Sham, L. J. (1965) *Phys. Rev. 140*, A1133.
15. Kohn, W. (1999) *Rev. Mod. Phys.* (Nobel Lecture) *71*, 1253.
16. Car, R. (2002) *QSAR 21*, 97.
17. Carloni, P., Rothlisberger, U., and Parrinello, M. (2002) *Acc. Chem. Res. 35*, 455.
18. Wu, X., Vargas, M. C., Nayak, S., Lotrich, V., and Scoles, G. (2001) *J. Chem. Phys.* 115, 8748.
19. Curti, B., Ronchi, S., and Simonetta, M. P. (1992) in *Chemistry and Biochemistry of Flavoenzymes* (Müller, F., Ed.) Vol. 3, Chapter 3, pp 69−94, CRC Press, Boca Raton, FL.
20. Mattevi, A., Vanoni, M. A., and Curti, B. (1997) *Curr. Op. Str. Biol. 7*, 804.
21. Palfey, B., and Massey, V. (1998) in *Comprehensive Biological Catalysis* Vol. 3, pp 83−154, Academic Press, Orlando.
22. Fitzpatrick, P. F. (2001) *Acc. Chem. Res. 34*, 299.
23. Mattevi, A., Vanoni, M. A., Todone, F., Rizzi, M., Teplyakov, A., Coda, A., Bolognesi, M., and Curti, B. (1996) *Proc. Natl. Acad. Sci. U.S.A. 93*, 7496.
24. Mizutani, H., Miyahara, I., Hirotsu, K., Nishina, Y., Shiga, K., Setoyama, C., and Miura, R. (1996) *J. Biochem. (Tokyo) 120*, 14.
25. Miura, R., Setoyama, C., Nishina, Y., Shiga, K., Mizutani, H., Miyahara, I., and Hirotsu, K. (1997) *J. Biochem. (Tokyo) 122*, 825.
26. Mizutani, H., Miyahara, I., Hirotsu, K., Nishina, Y., Shiga, K., Setoyama, C., and Miura, R. (2000) *J. Biochem. (Tokyo) 128*, 73.
27. Todone, F., Vanoni, M. A., Mozzarelli, A., Bolognesi, M., Coda, A., Curti, B., and Mattevi A. (1997) *Biochemistry 36*, 5853.
28. Umhau S., Pollegioni, L., Molla, G., Diederichs, K., Welte, W., Pilone, M. S., and Ghisla, S. (2000) *Proc. Natl. Acad. Sci. U.S.A. 97*, 12463.
29. Pollegioni, L., Fukui, K., and Massey, V. (1994) *J. Biol. Chem. 269*, 31666.
30. Pollegioni, L., Blodig, W., and Ghisla, S. (1997) *J. Biol. Chem. 272*, 4924.
31. Kurtz, K. A., Rishavy, M. A., Cleland, W. W., and Fitzpatrick, P. F. (2000) *J. Am. Chem. Soc. 122*, 12896.
32. Harris, C. M., Pollegioni, L., and Ghisla, S. (2001) *Eur. J. Biochem. 268*, 5504.
33. Fois, E., Gamba, A., and Tilocca, A. (2002) *J. Phys. Chem. B 106*, 4806.
34. Carter, E. A., Ciccotti, G., Hynes, J. T., and Kapral, R. (1989) *Chem. Phys. Lett. 156*, 472.
35. Hutter, J., et al. CPMD V3.5 (www.cpmd.org), copyright IBM Corp. 1990−2001, copyright MPI fuer Festkoerperforschung, Stuttgart, 1997−2001.
36. Troullier, N., and Martins, J. (1991) *Phys. Rev. B 43*, 1993.
37. Kleinman, L., and Bylander, D. (1982) *Phys. Rev. Lett. 48*, 1425.
38. Becke, A. D. (1988) *Phys. Rev. A 38*, 3098.
39. Perdew, J. P. (1986) *Phys. Rev. B 33*, 8822.
40. Nosé, S. (1984) *J. Chem. Phys. 81*, 511.
41. Röthlisberger, U. (1998) in *ACS Symposium Series* (Gao, J., and Thompson, M. A., Eds.) Vol. 712, Chapter 17, pp 264−274, American Chemical Society, Washington, DC.
42. Vanoni, M. A., Cosma, A., Mazzeo, D., Mattevi, A., Todone, F., and Curti, B. (1997) *Biochemistry 36*, 5624.
43. Hockney, R. W. (1970) *Methods Comput. Phys. 9*, 135.
44. Porter, D. J. T., Voet, J. G., and Bright, H. J. (1977) *J. Biol. Chem. 252*, 4464.
45. Sprik, M., and Ciccotti, G. (1998) *J. Chem. Phys. 109*, 7737.
46. Silvestrelli, P. L., Marzari, N., Vanderbilt, D., and Parrinello, M. (1998) *Solid State Commun. 7*, 107.
47. Boys, S. F. (1960) *Rev. Mod. Phys. 32*, 296.
48. Boero, M., Parrinello, S., Huffer, S., and Weiss, H. (2000) *J. Am. Chem. Soc. 122*, 501.
49. Miura, R., and Miyake, Y. (1987) *J. Biochem. 102*, 1345.
50. Pollegioni, L., Langkau, B., Tischer, W., Ghisla, S., and Pilone, M. S. (1993) *J. Biol. Chem. 268*, 13850.

BI020309Q